Molecular modeling of oxygen and water permeation in polyethylene

Anders Börjesson[ab], Edvin Erdtman*[a], Peter Ahlström[a], Mikael Berlin[c], Thorbjörn Andersson[c] and Kim Bolton[a]

[a] *School of Engineering, University of Borås, SE-501 90 Borås, Sweden. Tel:+46 33 435 4537; E-mail: edvin.erdtman@hb.se*

[b] *Present address: Combine Technology AB, Järntorget 4, SE-413 04 Göteborg.*

[c] *Tetra Pak Packaging Solutions AB, Ruben Rausings gata, SE-221 86 Lund, Sweden.*

Abstract:

Monte Carlo and molecular dynamics simulations were performed to calculate solubility, S, and diffusion, D, coefficients of oxygen and water in polyethylene, and to obtain a molecular-level understanding of the diffusion mechanism. The permeation coefficient, P, was calculated from the product of S and D. The AMBER force field, which yields the correct polymer densities under the conditions studied, was used for the simulations, and it was observed that the results were not sensitive to the inclusion of atomic charges in the force field. The simulated S for oxygen and water are higher and lower than experimental data, respectively. The calculated diffusion coefficients are in good agreement with experimental data. Possible reasons for the discrepancy in the simulated and experimental solubilities, which results in discrepancies in the permeation coefficients, are discussed. The diffusion of both penetrants occurs mainly by large amplitude, infrequent jumps of the molecules through the polymer matrix.

Introduction

The permeability of small penetrant molecules in polymer materials is important for many applications, *e.g.,* fuel cells[1], gas separation[2] and packaging[3]. Polyethylene (PE) is, for example, widely used for packaging materials and its barrier properties towards penetrants such as oxygen and water is a factor that determines the shelf-life of the packaged product. It is therefore important to identify the polymer properties that affect the permeation of penetrants. This will assist in developing new polymers and polymer composites that have desired barrier properties.

Experimental studies provide valuable understanding of the macroscopic[4-9] and microscopic[10, 11] properties of polymers and their transport properties. Michaels and co-workers[4, 5] found that there is a slight increase in the solubility of oxygen in polyethylene between 285 and 315 K, and that a further increase in temperature results in a far larger solubility. In contrast, Compañ *et al.*[12] found that the largest increase in solubility occurs at temperatures lower than 315 K, and that a further increase in temperature does not lead to a large increase in the solubility. Studies by Kurek *et al.*[9] yielded a decrease in solubility between 275 and 295 K, and a further increase in temperature leads to an increase in solubility. Experimental measurements of water solubility in PE or systems similar to PE are in better agreement. Schatzberg[13]

obtained an increase in solubility of water in *n*-hexadecane when increasing the temperature from 298 to 315 K, and McCall *et al.*[6] obtained a similar increase for water in PE over a larger temperature range of 298 to 335 K.

Experimental studies of diffusion of oxygen in PE[8, 9, 12] typically show an increase in diffusion coefficient with increasing temperature. These experiments have been conducted from 277 to 335 K, and the diffusion coefficients are $\sim 10^{-8} - 10^{-6}$ cm^2 s^{-1}. Similar results were obtained for water, where McCall *et al.*[6] obtained an increase in diffusion coefficient from 6×10^{-7} to 2×10^{-6} cm^2 s^{-1} between 306 and 333 K.

Computational simulations complement experimental studies by allowing easy manipulation and analyses at the molecular level. Insights gained at this level are expected to assist in identifying polymers with desired barrier properties. This has stimulated the development of a variety of computational techniques to calculate solubility and diffusion in polymers. These techniques can predict properties at both the macroscopic and molecular (microscopic) levels. At the macroscopic level it is possible to calculate diffusion[14-16] and solubility coefficients[14, 17, 18], and at the microscopic level it is possible to analyse properties such as clustering of the penetrant molecules[19], free volume[17] and rotations of polymer chains[20]. The work presented here illustrates the fact that a single model can provide properties at both the macroscopic and microscopic levels.

In contrast to experiments, where the permeation coefficient is determined from

$$P = \frac{\text{(quantity of penetrant)} \times \text{(film thickness)}}{\text{(area)} \times \text{(time)} \times \text{(pressure drop across film)}} \qquad (1)$$

it is common in simulations[21, 22] to determine the solubility coefficient[23], *S,* and diffusion coefficient, *D*, separately before calculating the permeation coefficient as,

$$P = S\,D \qquad (2)$$

Simulations are performed for a purely amorphous polymer phase, whereas experiments use polymer films with crystalline and amorphous regions. Differences between experimental and computational polymer material and measurement methods needs to be taken into consideration when comparing these data, and this is discussed in the Methods section.

The work presented here extends previous calculations of polymer transport properties by determining S, D and P for gas phase oxygen and liquid water in PE. Although it is possible to determine S using a variety of methods, including grand canonical Monte Carlo[24] (GCMC) and Henry's law method[21], the results presented below are obtained from the Gibbs ensemble Monte Carlo method[25, 26] (GEMC). This method was selected since the long term aim of this research is to perform a systematic study of transport properties over a variety of polymers, including hydrophobic and hydrophilic systems, where a large range of penetrant concentration will be studied. In addition, whereas the chemical potential is required GCMC simulations, a pressure is used as input in the GEMC technique. This simplifies comparison with experimental data, as well as the transfer of input parameters to the (*NpT*) molecular dynamics (MD) calculations. S and D are

therefore determined for the same system at the same conditions, which allows for the correct calculation of P. The pressure studied in this work is 1 atm and the temperatures are 278, 288, 298 and 308 K. These conditions are relevant, for example, to the packaging industry and mimic and range from refrigerator to hot room temperatures.

Methods

Force field

The AMBER (Assisted Model Building with Energy Refinement)[27], DREIDING[28], OPLS-AA (Optimized Potentials for Liquid Simulations – All Atom)[29] and CHARMM (Chemistry at HARvard Macromolecular Mechanics)[30] force fields have been successfully used to study polymeric systems[21, 31-33]. These models were therefore considered for the present study, and their validity were tested for the PE system studied here. The tests focused on the polymer density (although other properties such as melting and glass transition temperatures are also important), since this is expected to be a critical property for the permeation of molecules through the polymer. For example, if the force field yields a density that is too low, then there will be more free volume that can be occupied by the penetrant, hence increasing S and perhaps D (and hence P).

The initial density simulations were performed using *n*-octane (which has a similar structure to PE) since these systems require far less computational time to equilibrate. One of the force fields that gave the proper density for *n*-octane (AMBER) was then used to calculate the density of PE which, as discussed below, was also in agreement with experiment. This force field was therefore used in the MC and MD simulations to determine S and D.

A second reason for choosing the AMBER force field is that one can include atomic charges[27] using, for example, the restrained electrostatic potential (RESP) method[34]. This was done using *n*-dodecane as a model of PE, and the R.E.D. code[35] (RESP and ESP charge Derive) in conjunction with Gamess-US[36]. As discussed below, this method yielded very small atomic charges, which is reasonable since *n*-dodecane (and PE) molecules do not contain highly electronegative groups.

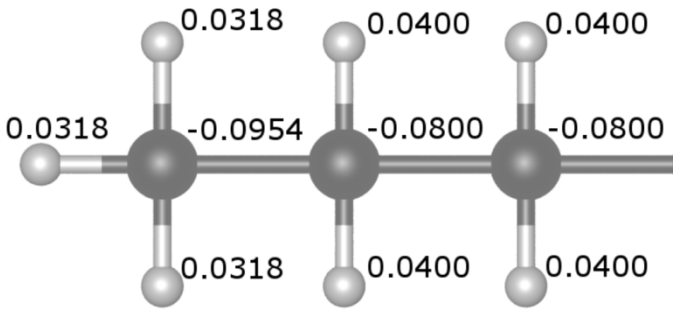

Figure 1: The AM1-BCC charges for terminal CH_3 and interior CH_2 units of PE

An alternative to the computationally demanding RESP charge calculations is the AM1-BCC[37, 38] scheme which is designed to mimic the RESP charges but is based on bond charge corrected semi-empirical

AM1 Mulliken charges instead of Hartree-Fock charge density. This method was also examined, and the AM1 charges were calculated using Mopac[39] for 20 different structures of *n*−octane. The final atomic charge was obtained by averaging over all 20 structures and ensuring neutrality of each methylene unit. These charges, which are shown in Figure 1, are larger than the charges obtained from the RESP method and were therefore included in the AMBER force field to test their effect (*i.e.*, simulations were performed with and without atomic charges to ascertain their importance).

The force field of Fischer and Lago[40] was used for the oxygen molecules, and the modified TIP3P force field [41] was used for the water molecules. The modified TIP3P force field includes Lennard-Jones terms for the hydrogen atoms which improves the simulation results, especially when Ewald summation methods are used.[42]

Polymer structures

Although it is, in principle, possible to obtain S and D from single, long simulations, the long-time dynamics of the polymer chains makes this an extremely resource intensive approach. An alternative is to simulate an ensemble of trajectories, where each trajectory is performed using a polymer matrix that is significantly different from the matrices used in the other trajectories, but that is still representative of the polymer structure at the given temperature and pressure.

The initial PE matrices were created by randomly inserting six PE chains of 200 carbon atoms each in a cubic simulation box with 45Å sides. Previous studies[43] have shown that this number of chains is sufficiently large, and that the chains are sufficiently long, to provide converged results for PE. These structures were constructed using the grand canonical Monte Carlo (GCMC) method with a chemical potential that was sufficiently large to induce the six PE chains into the box while at the same time avoiding large atomic overlaps.

The box was then compressed until the sides were 30Å, which corresponds to a PE density of approximately 1 kg/L. This is far larger than the experimental value of ≈ 0.855 kg/L[44] for amorphous PE, and allowed for efficient inter- and intra-chain relaxation. Thirty-two statistically independent PE matrices were constructed using this procedure, and these structures were then equilibrated using MD simulations in the *NVT* ensemble for more than 1 ns at a temperature of 680 K. This is well above the PE melting point and together with the large density, allowed for efficient equilibration of the initial structures. The temperature was then gradually decreased to the desired temperature (278, 288, 298 or 308 K) over a 2 ns simulation. As a final equilibration step, the structures were simulated for 4 ns in the *NpT* ensemble at the desired temperature and a pressure of 1 atm. This procedure yielded equilibrated PE matrices for all of the 32 structures, as seen by constant average densities and potential energies.

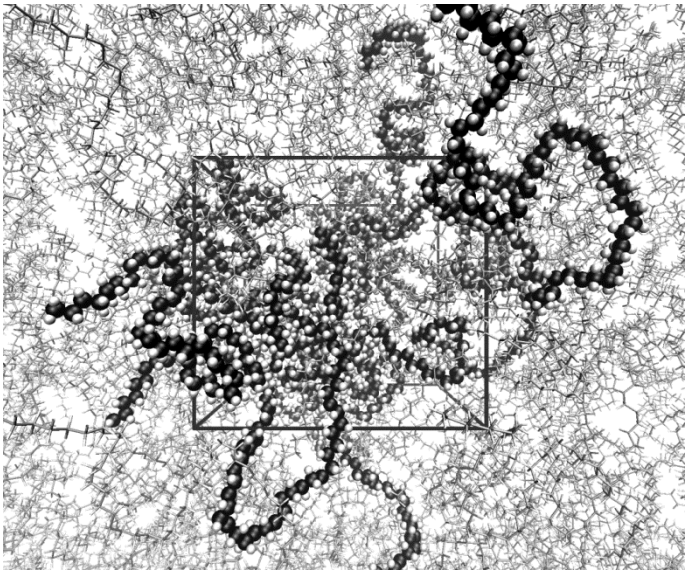

Figure 2: A typical PE matrix containing six polymer chains, each having 200 C atoms. The ball-and-stick model represents the PE chains with their centre of mass in the unit cell and the thin-line model represents their periodic replicas.

To further increase the number of trajectories in each ensemble, each of the 32 structures were simulated for an additional 1 ns at the desired temperature and pressure, and matrices were collected every 0.25 ns, *i.e.,* after 4.25, 4.5, 4.75 and 5.0 ns. These 4×32 structures comprised the ensemble of 128 trajectories to calculate S and D at each temperature. A typical structure is shown in Figure 2. The periodic simulation cell is indicated by the straight solid lines, the ball-and-stick model represents the PE chains with centre of mass in the unit cell and the thin line model represents the periodic replicas.

Simulation methods

MC simulations were performed with the MCCCS (Monte Carlo for Complex Chemical Systems) Towhee computer program[45] and MD simulations with the LAMMPS (Large-scale Atomic/Molecular Massively Parallel Simulator)[46, 47] software. There are several reasons for this. First, all simulations that are required to calculate P for a penetrant in a polymer matrix can be done with these two programs. Second, the programs are highly compatible. For example, they contain many force fields that are common to both programs, and force field modifications and topology files that are made for the MCCCS Towhee program are readily transferred to the LAMMPS software. Third, both programs are included in the commercial, user-friendly platform MAPS[48] which, in principle, makes it easier to use this platform for similar studies.

As discussed above, the validity of each force field was tested by determining the density of *n*-octane and PE systems and comparing the calculated densities with experimental data. For n-octane, 110 molecules where placed in a 30×30×30 $Å^3$ periodic box and 8 parallel simulations were performed for at least 3.5 million MC steps. For PE, the system described in the previous section was used in a MD simulation in the *NpT* ensemble. The systems were equilibrated when the average density and potential energy were constant.

Calculations to determine S were performed using MC simulations in the Gibbs *NpT* ensemble[25, 26]. One of the simulation boxes contained the PE matrix and the other box contained either gaseous oxygen or

liquid water. The gas/liquid phase box contained either 200 O_2 molecules or 1000 H_2O molecules. This system size has successfully been used in previous simulations of the solubility of water in PE.[43] Since oxygen and water have low solubilities in PE under the conditions studied here, the PE matrix is not expected to show significant swelling, and the volume of the PE box was fixed to decrease the simulation time. For comparison, some simulations were also performed with flexible volume of the PE box. However, the simulation speeds were up to 18 times slower (largest difference for the oxygen system), and there were no significant changes in the results.

The probability of selecting a specific MC move is: 0.01 for *NpT* volume change of the gas/liquid phase, 0.01 for O_2 or H_2O transfer between boxes, 0.48 for atomic displacements on any atom in any box, 0.25 for centre of mass displacement of O_2 or H_2O and 0.25 for centre of mass rotation of O_2 or H_2O. For the oxygen simulations, 85×10^6 MC moves were performed for each trajectory in the ensemble. For the water simulations, 29×10^6 MC moves were typically performed for each trajectory. Less MC moves were attempted for the water system due to its increased computational expense. This stems from the water system being significantly larger, containing approximately 7600 atoms instead of approximately 4000 atoms for the oxygen systems. There are also a larger number of charge-charge interactions in the water system. The systems were assumed to be equilibrated when there were a constant average number of penetrant molecules in the PE simulation box.

The solubility of a penetrant in a polymer can be given in different ways and with different units (*e.g.* mg(penetrant) / g(polymer) or mol(penetrant) / mol(polymer))[43]. The solubility coefficient that is used to determine the permeation coefficient is the partition function of the penetrant molecules in the polymer, *i.e.*, the ratio between the number of penetrant molecules in the polymer box and the number of these molecules that would have been in this box in the absence of the polymer. This is calculated by determining the average number of penetrant molecules in the PE box, and dividing by the number of molecules that would have been in this box in the absence of the polymer. This is the same as:

$$S = \frac{\text{(effective volume of pentrant molecules in PE box)}}{\text{(volume of the PE box)}} \tag{3}$$

where the (effective volume of penetrant molecules in PE box) is the volume that the absorbed molecules would have in the penetrant box.

The units are therefore $cm^3\ cm^{-3}$, which are used in the results presented below. It is important to note that the density of the molecules in the penetrant box, ρ(penetrant box), can be determined explicitly from the simulations, which is another motivation for using the GEMC method. As discussed below, additional conversions are required to compare experimental data with the simulated results.

For the equilibrium MD calculations, D was determined from simulations performed in the *NpT* (equilibration) and *NVT* (production) ensembles using the Nose-Hoover method with damping parameters of 0.1 ps and 10 ps for the thermostat and barostat, respectively. The equilibration simulations in the *NpT*

ensemble were performed until the density was constant, which was obtained after 2.5 to 5.0 ns. The *NVT* production simulations were then performed for at least 3.5 ns. The time step was 1 fs and integration was performed using the Verlet algorithm, which has the strength of being time-reversible.[49]

The diffusion coefficient (D) in three dimensions is determined from the equilibrated system using[50]:

$$D = \frac{1}{6} \frac{\Delta \, \mathrm{MSD}(t)}{\Delta t} \tag{4}$$

where Δ indicates the change in mean square displacement (MSD) of time (*t*). MSD is defined as:

$$MSD(t) = \langle |\boldsymbol{r}(t) - \boldsymbol{r}(0)|^2 \rangle \tag{5}$$

where *r(t)* is the penetrant's position at time *t, r(0)* is its initial position and <…> denotes the ensemble average. Hence, D is determined from the slope of the MSD as a function of time. The simulations were sufficiently long (at least 3.5 ns) to obtain a linear increase in the MSD over time. Hence, MSD $\propto t^{\alpha}$, with $\alpha = 1$, which reveals that the penetrant moves via diffusion (and not subdiffusion [51, 52]) and the motion is therefore described by Eq. 4.

As discussed below, diffusion of oxygen and water in PE is dominated by infrequent hopping events, and hence rather long MD trajectories need to be propagated to obtain statistically converged results. As a comparison, the non-equilibrium MD (NEMD) method was used in this work. The penetrant is pulled through the polymer matrix during an MD-simulation to measure the friction coefficient *v*.[53, 54] The pulling is performed by adding a spring potential between the origin and the centre of mass of the penetrant molecule. According to the Langevin equation the following is true in the overdamped limit, *i.e.* when $v/m \gg \sqrt{k/m}$ [53]:

$$\langle R(t) \rangle = R_0 \, e^{-(2kt/v)} \tag{6}$$

where *m* is the mass of the penetrant, *k* is the spring constant, *R(t)* and R_0 are the distances between the molecule and the origin at time *t* and time $t = 0$, respectively and <…> denotes the ensemble average over 128 trajectories. Hence, the friction coefficient is obtained from the slope of $\ln\langle R(t) \rangle$ against time. D is subsequently obtained from Einstein's relation:

$$D = k_B T / v \tag{7}$$

where k_B is Boltzmann's constant and *T* is the temperature.

The NEMD trajectories were propagated for 150 ps, with spring constants $k = 3.474 \times 10^{-4}$ and 6.948×10^{-4} kg s^{-2}. Comparison with the equilibrium MD results (presented below) showed that the lower spring constant is sufficiently small to yield a converged value for D. The computational time for each NEMD simulation was a factor of 25 cheaper than an equilibrium MD simulation.

Due to their low solubilities in PE, there is on average less than one oxygen or water molecule in the polymer box during the GEMC simulations. That is, there is no penetrant molecule in the PE matrix in many

of the MC steps. Based on these results, the MD simulations were performed with only one penetrant molecule in the PE matrix. In an attempt to obtain statistical convergence in a shorter computational time, more penetrant molecules were included in the polymer matrix. However, when as little as 8 water molecules were added to the PE matrix there was a decrease in the diffusion coefficient by almost 50%. A radial distribution analysis of the water molecules showed that this was due to the formation of water clusters. This has also been reported elsewhere.[19] Although this problem was not observed for oxygen, all results presented below are from simulations where only one penetrant is included in the PE matrix.

The error bars given in figures below show a 95% confidence interval and are obtained from the bootstrap method[55, 56]. 10000 average values are determined from sets of 128 randomly selected trajectories with replacement, and the 95% confidence interval was determined from these average values.

Comparison between simulated and experimental results

Experimental studies often give the solubility coefficients of gaseous penetrants in units of cm^3(STP) cm^{-3} $cmHg^{-1}$. In order to compare with our results, the conversion is[57]:

$$S^*\left(\frac{cm^3}{cm^3}\right) = S^*_{meas}\left(\frac{cm^3_{STP}}{cm^3\ cmHg}\right) \times \frac{T}{T_0} \times \alpha_p \tag{8}$$

$$P^*\left(\frac{cm^2}{s}\right) = P^*_{meas}\left(\frac{cm^3_{STP}\ cm}{cm^2\ s\ cmHg}\right) \times \frac{T}{T_0} \times \alpha_p \tag{9}$$

where S^* is the experimental converted solubility coefficient and and S^*_{meas} the experimentally measured solubility coefficient. T is the experimental temperature, T_0 the temperature at STP (*i.e.* 273 K), and α_p is the pressure conversion factor (*e.g.* 76 cmHg). Similarly, P^* and P^*_{meas} are the converted and measured experimental permeability coefficients.

Conversion of experimental results for liquids is usually simpler since the solubility coefficient is usually given as ppm, *i.e.*, μg(penetrant) g(polymer)$^{-1}$. One simply converts to cm^3 cm^{-3} by multiplying with the density of pure polymer divided by the density of pure penetrant.

Comparison of the simulated results with experimental data is also hampered by other factors. As discussed in the Introduction, one factor is the large variation in the experimental results. A second factor is the presence of impurities in experimental samples which can affect the solubility coefficient[58, 59] and probably also the diffusion coefficient. In principle, one can investigate the effect of such impurities by including them in the simulations, but this requires the identification of 'typical' impurities and is beyond the scope of this study.

A third factor is that there are crystalline regions in the PE samples used in experiments, whereas the simulations are done on amorphous PE matrices. The crystalline regions are too large to include in molecular-level simulations, and one needs to correct for the degree of crystallinity. Assuming that no penetrant is absorbed in the crystalline regions (and hence also that diffusion occurs only in the amorphous phase), Michaelis *et al.*[4, 5, 23] proposed the following conversion equations:

$$S = S^*/\chi_{am} \tag{10}$$

$$D = D^* \tau \beta \tag{11}$$

where S^* and D^* are the experimentally determined solubility and diffusion coefficients, χ_{am} is the fraction of amorphous regions in the sample, τ is a geometric impedance factor which accounts for the decreased diffusion when the penetrants need to find a route around the crystal regions, and β an immobilization factor for the polymer chains due to the presence of the crystal regions.

From equations 2, 10 and 11 the permeability coefficient is:

$$P = \frac{S^* D^* \tau \beta}{\chi_{am}} = \frac{P^* \tau \beta}{\chi_{am}} \tag{12}$$

where P^* is the experimentally determined permeation coefficient.

Table 1 Fractions of amorphous region χ_{am} from experiments used to compare with simulation data.

Reference	χ_{am}
[4, 5]	0.23[a]
	0.57[a]
[60]	0.396
	0.392
	0.386
[61]	1[a]
[12]	0.75
[8]	0.69
[9]	0.740
	0.706
	0.684
	0.686
[6]	0.500[b]
[13]	1[c]
[62]	0.479[b]
[63]	0.514[b]
	0.493[b]

[a] The numbers given are for calculation of D and P, but χ_{am} = 1 was used for calculation of S, since crystallinity was already accounted for in the reference.
[b] Not given explicitly in reference, but calculated from density.
[c] Crystallinity neglected due to short chains.

Pant and Boyd[16] used a simpler conversion for the diffusion coefficient which was derived from an expression for the dielectric tensor[64]. With the assumption that diffusion in the crystalline regions is negligible, the diffusion coefficient is:

$$D = \frac{3}{2}\frac{D^*}{\chi_{am}} \tag{13}$$

and hence:

$$P = \frac{3}{2}\frac{P^*}{\chi_{am}^2} \tag{14}$$

It may be noted that, in the work presented here, experimental data are converted into an ideal fully amorphous system by equations 10, 13 and 14, to allow for comparison with simulation results, and not *vice versa*, since this allows for comparison with samples that have differing degrees of crystallinity. The χ_{am} values that were used in the conversion are given in Table 1.

Temperature dependence

The calculated values of S at different temperatures enables one to determine the heat of solution (ΔH_S) from the van't Hoff equation:

$$ln\, S = ln\, S_0 - \frac{\Delta H_S}{R}\frac{1}{T} \quad (15)$$

where S_0 is the pre-exponential factor and R is the gas constant. The activation energies of diffusion (E_D) and permeability (E_P) can be calculated in an analogous manner from the Arrhenius equation:

$$ln\, D = ln\, D_0 - \frac{E_D}{R}\frac{1}{T} \quad (16)$$

$$ln\, P = ln\, P_0 - \frac{E_P}{R}\frac{1}{T} \quad (17)$$

where D_0 and P_0 denote pre-exponential factors.

Hence, the heat of solutions and activation energies were calculated from the slope of the natural logarithm of S, D and P against the reciprocal temperature.

Results and Discussion

Force field

The AMBER, OPLS-AA and CHARMM force fields yielded *n*-octane densities at 298 K and 1 atm of 0.693, 0.693 and 0.697 g cm^{-3}, respectively, which all are in reasonable agreement with the experimental density[65] of 0.699 g cm^{-3}. The Dreiding force field yielded a density of 0.595 g cm^{-3}, which is ~15% lower than experiment. Hence, the first three force fields may provide valid descriptions for alkane-like polymer systems, whereas these initial calculations indicate that the Dreiding force field may provide densities that are too low. This was confirmed by performing simulations of PE at 1 atm and 298 K, where it was seen that the Dreiding force field yielded a density of ~0.7 g cm^{-3}, which is ~20 % lower than the experimental density[44] of 0.855 g cm^{-3}. Hence, the deficiencies seen for *n*-octane were transferred to PE and no further studies were performed using this force field.

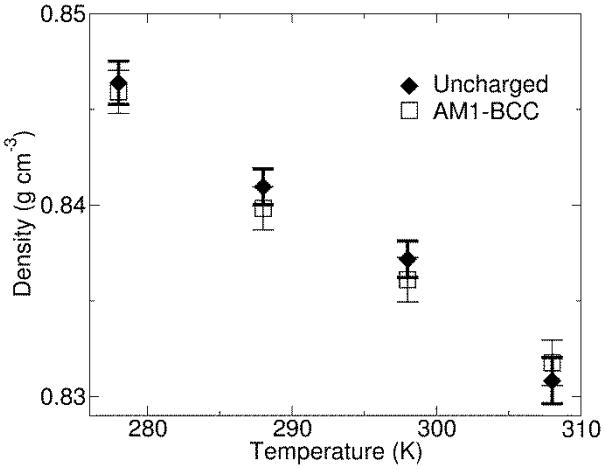

Figure 3: Density of PE without charges (filled diamonds with bold error bars) and with AM1-BCC charges (open squares with thin error bars) at 1 atm and from 278 K to 308 K. The error bars indicate a 95% confidence interval.

The AMBER force field was selected as a candidate from the remaining three force fields since, as discussed above, there are well documented procedures to calculate atomic charges and include them in the force field.[24, 25, 34] This may be important when calculating S and D for penetrants that have large dipole moments (such as water). The densities for PE at 1 atm and from 278 K to 308 K were calculated with the AMBER force field are given in Figure 3. As mentioned above, this force field yields densities that are similar to the experimental data for amorphous PE and it also yields the expected trend of decreasing density with increasing temperature. Since this force field yielded valid polymer densities, it was used in subsequent calculations. The OPLS and CHARMM force fields were not used although they may also provide a valid description of the PE system.

As described above, both the RESP and the AM1-BCC methods were used to obtain atomic charges for the PE chains. The RESP method yielded charges that were smaller than the AM1-BCC method. For example, the magnitude of the atomic charges for the non-terminal methylene groups were less than 0.015 *e*, and the C atoms on the terminal methyl groups had slightly higher charges of −0.08 *e*. The AM1-BCC atomic charges were larger and are shown in Figure 1. Hence, only the AM1-BCC charges were used to investigate the effect of these charges on the polymer structural and barrier properties. It is evident from Figure 3 that including these atomic charges has a marginal effect on the PE density.

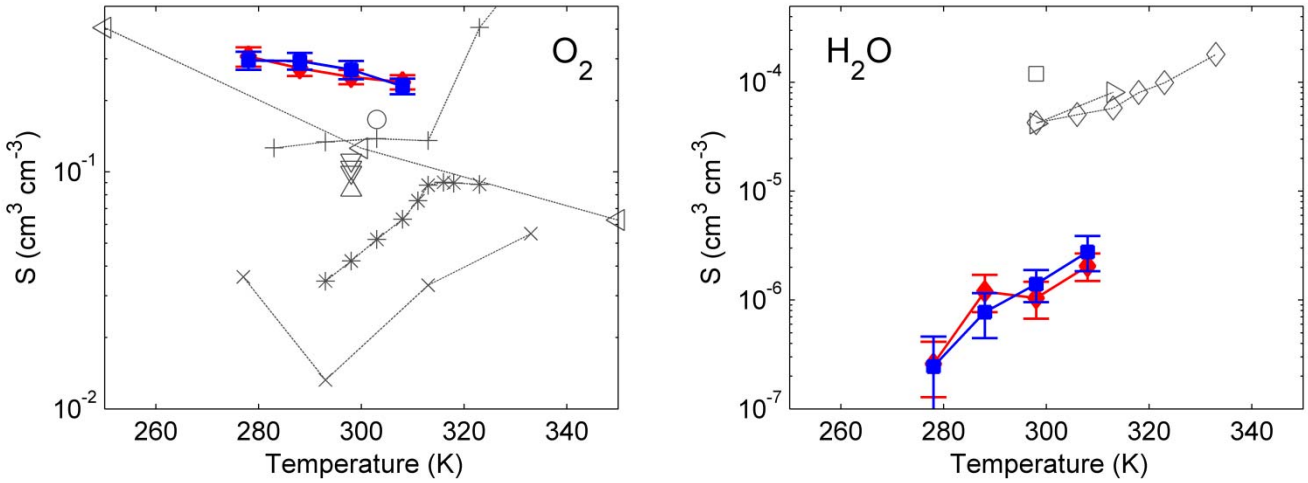

Figure 4: Simulated and experimental solubility coefficients in logarithmic scale of oxygen (left) and water (right). Simulated (this work) S coefficients are shown with bold solid lines and filled symbols, where uncharged and charged PE is represented by red diamonds and blue squares, respectively. The error bars indicate the 95% confidence interval. Other studies are shown in grey and refers to: another simulation study (◁)[14], and experimental studies (△)[4, 5], (▽)[60], (○)[61], (✳)[12] , (+)[8], (×) [9], (◇)[6], (▷)[13] and (□)[62]. The experimental data are converted using equation 10 and the factors in Table 1

Solubility

Figure 4 shows simulated and experimental solubility coefficients for oxygen and water in PE at 1 atm and temperatures from 278 K to 308 K.

The simulated solubility coefficient for oxygen in uncharged PE decreases from 0.30 ± 0.03 $cm^3\ cm^{-3}$ (0.51 ± 0.05 $mg_{oxygen}/g_{polymer}$) at 278 K to 0.24 ± 0.02 $cm^3\ cm^{-3}$ (0.37 ± 0.04 $mg_{oxygen}/g_{polymer}$) at 308 K. The corresponding numbers for charged PE are 0.30 ± 0.04 $cm^3\ cm^{-3}$ and 0.23 ± 0.02 $cm^3\ cm^{-3}$, respectively, showing that the inclusion of atomic charges in the force field does not significantly affect the solubility coefficients. Hence, possible changes in the PE matrix due to the additional chain-chain interactions caused by these changes are not sufficiently large to affect the oxygen solubility coefficient. Although the simulated coefficients are in the same order of magnitude of some experimental studies[4, 8, 60, 61] they are larger than the data obtained in other studies[9, 12]. The simulations also yield decreasing S with increasing temperature, which is in agreement with experimental data that shows a decreasing trend in certain temperature intervals[8, 9], but is not in agreement with some other experimental studies. This decreasing trend is also seen in another computational study[14] of amorphous PE.

The solubility of water in PE ranges from (0.26 ± 0.16) × 10^{-6} $cm^3\ cm^{-3}$ (0.32 ± 0.19 $\mu g_{oxygen}/g_{polymer}$) at 278 K to (2.05 ± 0.63) × 10^{-6} $cm^3\ cm^{-3}$ (2.6 ± 0.8 $\mu g_{oxygen}/g_{polymer}$) at 308 K. Hence, the solubility of water increases with temperature, a trend that is in agreement with the experimental data, although the simulated results are one order of magnitude lower.[6, 13] As for oxygen, it is evident from Figure 4b that the inclusion of charges does not significantly affect the values of S for water (when including charges S = (0.25 ± 0.21) × 10^{-6} $cm^3\ cm^{-3}$ at 278 K and S = (2.77 ± 1.12) × 10^{-6} $cm^3\ cm^{-3}$ at 308 K). The solubility of water is up to six orders of magnitude lower than that of oxygen. This is primarily due to the fact that the bulk phase of oxygen is gas and for water it is liquid. Hence the effective volume of water in the polymer is far smaller

than that of oxygen. Analysis of the penetrant molecules in the PE matrix shows that the average number of water molecules in the polymer matrix is one order of magnitude lower than that for oxygen. This explains why, even though long simulations were performed, the errors obtained for water are larger than those for oxygen.

As shown above, the solubility coefficient of oxygen decreases with increasing temperature whereas that of water increases. This is probably due to the different phases of the penetrant outside the polymer matrix, *i.e.*, oxygen is in the gas phase and water is liquid. An increase in temperature increases the kinetic energy of the penetrant in the polymer (and in the penetrant bulk phase) which, in turn, increases the volume required by the penetrant. Hence, gas phase penetrants may prefer to desorb from the polymer into the gas phase, whereas the much smaller free volume in the liquid bulk phase hinders desorption.

Diffusion

Figure 5 shows three typical MSD curves for a single oxygen molecule dissolved in PE at 308 K and 1 atm, as well as the ensemble average over the 128 trajectories. Examination of the MSDs from single molecules provides valuable information about the diffusion process and the importance of having a large number of trajectories in the ensemble in order to get statistically converged results. Since the diffusion coefficient is obtained from the slope of the MSD, it is clear that a single 3.5 ns trajectory cannot provide converged data. The results presented here show that statistical convergence is obtained from 128 independent trajectories, each 3.5 ns long.

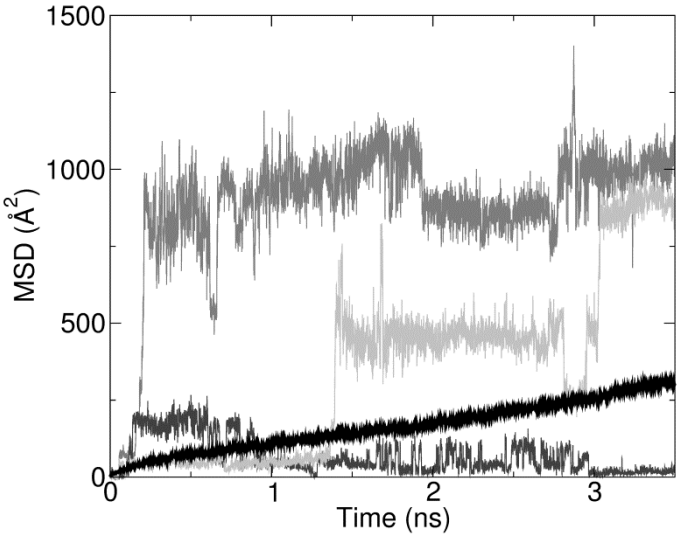

Figure 5: Three typical MSDs of an oxygen molecule in PE at 308K. The average MSD, shown in black, reveals a linear increase in MSD with time.

The MSDs of single oxygen molecules show a variety of behaviours, from almost no diffusion through molecules that show several smaller jumps to molecules that show very large jumps that result in changes in MSD by almost 1000 Å^2. It is also evident that the MSD is fairly constant between the jumps. This indicates that diffusion is dominated by successive jumps between regions in the polymer. This could either be due to the oxygen jumping between voids in the polymer matrix, or the motion of the polymer chains annihilating

and creating voids in the matrix, or a combination of these processes.

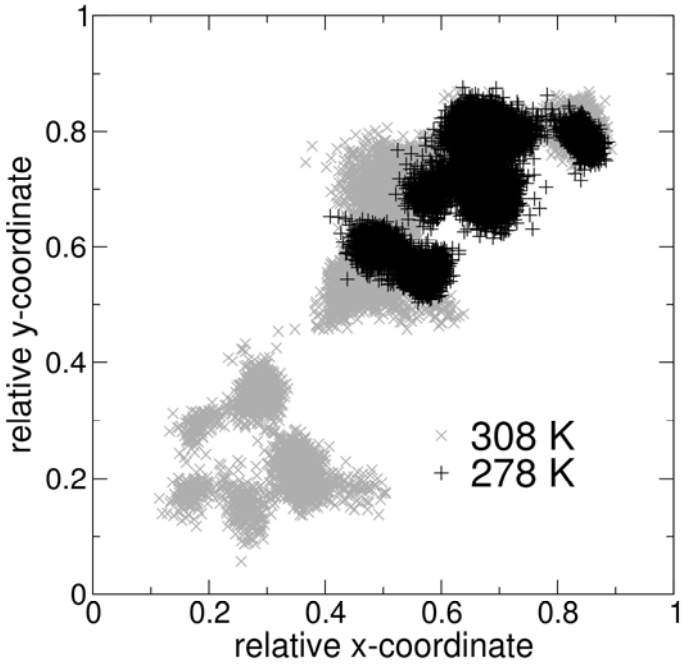

Figure 6: Typical trajectories of an oxygen molecule diffusing in PE projected onto the xy-plane. The positions were sampled every 0.5 ps over a total simulation time of 4 ns. Data are given for temperatures 278 K (black plusses) and 308 K (grey crosses).

The jumps of the molecules is further illustrated in Figure 6, where the oxygen positions monitored over single trajectories at 278 and 303 K are projected onto the *xy*-plane. At the lower temperature the penetrant remains in three distinct regions, with little or no sampling in the area between these regions. This would be reflected by two single jumps and three constant regions in the MSD curve (or possibly several jumps between the constant regions). The oxygen molecule in the trajectory at 308 K has positions that cover a far larger region of coordinate space, jumping between regions and showing sampling between these regions.

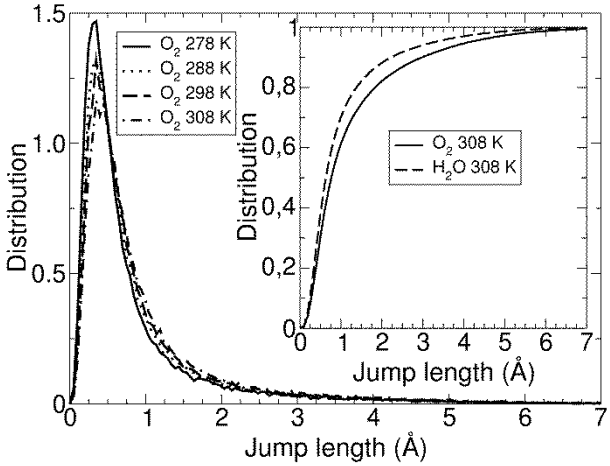

Figure 7: Distribution of diffusion jump lengths of oxygen in uncharged PE at different temperatures. Inset: Cumulative distribution of jump lengths in uncharged PE of oxygen (solid line) and water (dashed line)

Fig. 7 shows the distribution of the jump lengths of the oxygen molecule in the uncharged PE matrix at different temperatures. The jump lengths were calculated in the following manner: The average of the penetrant's centre of mass was calculated over 10 ps intervals along the trajectory. The jump length was then

defined as the distance between two adjacent intervals[16]. The distributions in Fig. 7 were obtained from the 128 trajectories in the ensemble for each temperature, and areas under the curves are normalized to unity to allow for comparison. It was found that the inclusion of charges in the force field does not significantly alter the results. In agreement with the data shown in Figure 6, an increase in temperature results in a larger number of longer jumps.

The diffusion mechanism for water in PE is very similar to that discussed above for oxygen. The insert of Fig. 7, which shows the normalised cumulated number of jumps less than a given length, shows that the cumulative distribution for water is similar to that for oxygen, but with the difference that there are a larger number of smaller jumps for water than for oxygen.

One of the reasons for the shorter jumps observed for water may be the difference in the molecular sizes of oxygen and water. For the oxygen molecule, the Lennard-Jones (LJ) diameter of each atom is 3.09 Å, and the O=O oxygen minimum energy bond length is 1.0166 Å. For the water molecule the oxygen and hydrogen LJ diameters are 3.1506 Å and 0.4000 Å, respectively, the O-H bond length is 0.9572 Å and the H-O-H angle is 104.52 degrees. The length of the oxygen molecule is hence approximately 4.1066 Å and the diameter of the water molecule is approximately equal to the LJ diameter of the oxygen atom (3.1506 Å). Hence, the smaller size of the water molecule may allow it to jump to voids that are not accessible to the oxygen molecule.

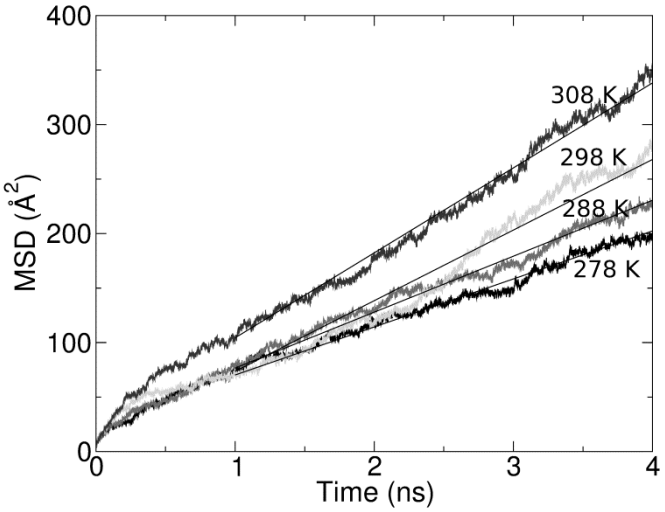

Figure 8: Average MSD of oxygen in uncharged PE at different temperatures with the estimated slope shown by straight solid lines.

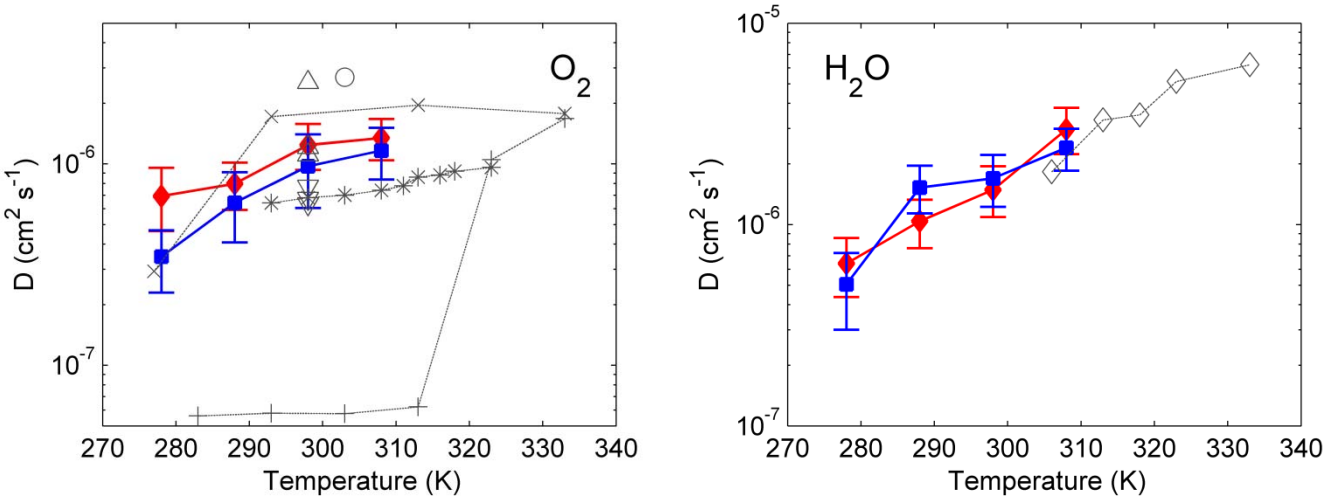

Figure 9: Simulated and experimental data of the diffusion coefficients in logarithmic scale of oxygen (left) and water (right). The symbols are the same as those in Figure 4. The experimental data are converted using equation 13 and the factors in Table 1.

Fig. 8 shows the MSDs of the oxygen molecule in PE averaged over the 128 trajectories at 1 atm and temperatures of 278, 288, 298 and 308 K. The straight lines are best fits to the linear regions of the MSD curves. These linear fits, as well as those obtained for water in PE, were used to calculate the diffusion coefficients shown in Fig. 9. The figure includes data from simulations based on the neutral PE chains (filled red diamonds) and PE with AM1-BCC charges (filled blue squares) as well as experimental data corrected for the crystallinity.

It is evident from Fig. 9 that, similar to all properties discussed above, the inclusion of atomic charges in the force field does not have a large effect on the diffusion coefficients. For example the largest difference is found for oxygen at 278 K, where D in charged PE is $(0.35 \pm 0.13) \times 10^{-6}$, while that of uncharged PE is $(0.69 \pm 0.27) \times 10^{-6}$. These results are statistically the same (the error intervals overlap).

The simulated diffusion coefficient for oxygen (in uncharged PE) increases from $(0.69 \pm 0.27) \times 10^{-6}$ $cm^2\ s^{-1}$ at 278 K to $(1.3 \pm 0.4) \times 10^{-6}$ $cm^2\ s^{-1}$ at 308 K. The diffusion coefficients of water are very similar, and increases from $(0.6 \pm 0.3) \times 10^{-6}$ $cm^2\ s^{-1}$ at 278 K to $(3.0 \pm 0.8) \times 10^{-6}$ $cm^2\ s^{-1}$ at 308 K Comparison between the simulated and experimental data shows that both results give the same trends and are in qualitative or even semi-qualitative agreement. For both penetrants the diffusion coefficient increases with temperature. The simulated diffusion coefficients for oxygen are in agreement with experiment although, due to the large divergence in experimental data, there is also disagreement with some of the experimental data. The simulated D for water is in very good agreement with all of the available experimental data.

Fig. 9 also shows that the simulated diffusion coefficients for water are slightly larger than those for oxygen (at least at the higher temperatures). This trend is in agreement with the experimental data and may, at least partially, be explained by the larger size of the oxygen molecules compared to the water molecules discussed above.

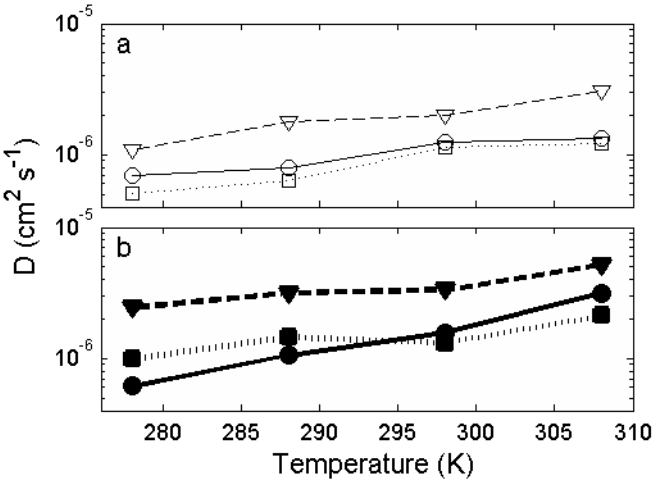

Figure 10: NEMD diffusion simulations of a) oxygen and b) water in PE at two different spring constants (triangles: k = 6.95 × 10^{-4} kg s^{-2}, squares: k = 3.47 × 10^{-4} kg s^{-2}) in comparison with diffusion coefficients calculated from MSD (circles).

NEMD results

The NEMD calculations were approximately a factor of 25 faster than the MD simulations required to obtain the MSD. The results obtained for oxygen and water are shown in Fig. 10 for force constants of 6.948 × 10^{-4} kg s^{-2} and 3.474 × 10^{-4} kg s^{-2}. The results obtained from the MSD calculations are also shown in Fig. 10 for comparison. The higher force constant gave a higher D than the MSD method, which is probably due to the fact that the PE chains do not have time to relax, when the penetrant is pulled through the matrix. It is, however, clear that there is good agreement between the D obtained from the NEMD method with the lower spring constant and that obtained from the MSD curve. Hence, the NEMD method may be preferred for these types of simulations, although further validation is required for other polymers, both above and below their glass transition temperatures.

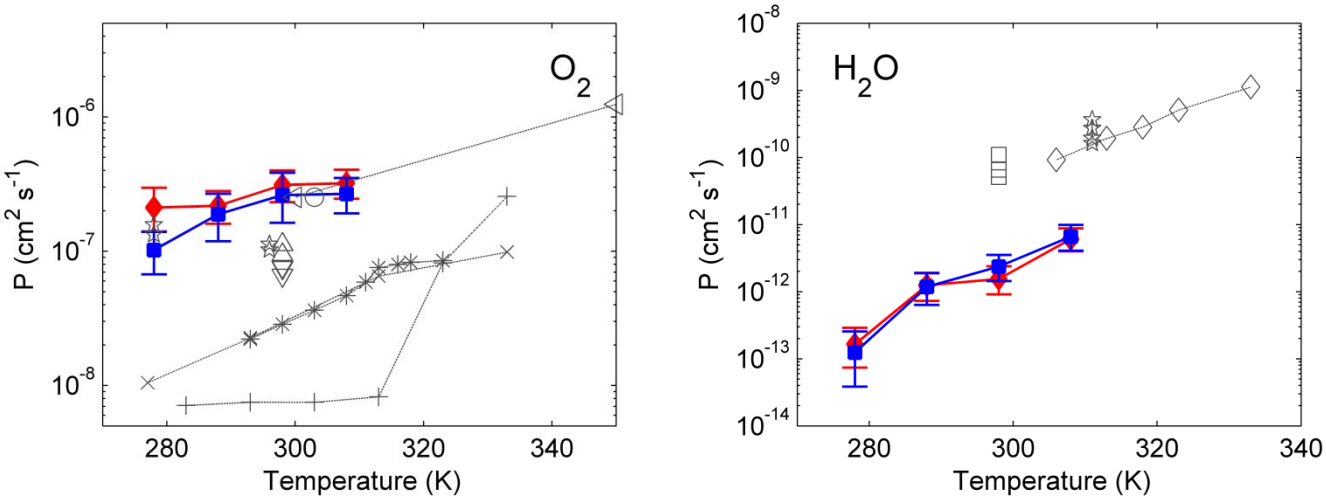

Figure 11: Calculated and experimental permeability coefficients in logarithmic scale of oxygen (left) and water (right). Besides the symbols given in Figure 4, ✯ is taken from ref. [63]. The experimental data are converted using equation 14 and the factors in Table 1.

Permeation

Fig. 11 shows the simulated permeation coefficients for oxygen and water in PE at 1 atm and 278, 288, 298 and 308 K. Since S and D were not affected by the partial charges of the PE chains, P is not significantly affected either, as seen in Fig. 11. The permeation coefficient increases over this temperature range for both penetrants, with oxygen showing a ~200% increase and water ~5000 % increase. Hence, whereas P for oxygen is three orders of magnitude larger than P for water at 278K, it is only two orders of magnitude larger at 308 K. This is due to the higher permeation activation energy for water in PE, which is discussed below.

The experimentally determined permeation coefficients for oxygen in PE are 1.1×10^{-7} cm^2s^{-1} and 9.4×10^{-8} cm^2s^{-1} for low density PE (LDPE) and high density PE (HDPE) at 1 atm and 298 K, respectively,[5, 66] which is shown with △ symbols in Fig. 11 together with other experimental data. Note that the values from experiments in Fig. 11 are the values after removing the effect of the crystallinity (using equation 14 and the factors from Table 1), and should therefore be equal. As discussed above, this indicates that this equation is not sufficient for taking the effect of crystallinity into account and/or that there are other important factors, such as the introduction of impurities into the PE matrix during processing, that affect the permeation coefficient. However, the permeation coefficient estimated from extrapolation to 100% amorphous PE from a large amount of experimental data in the range 298-308 K and 1–10 atm is found to be 2.5×10^{-7} cm^2s^{-1} (○ in Fig. 11).[61] This value agrees well with the simulated values of $(3.2 \pm 0.9) \times 10^{-7}$ cm^2s^{-1} (uncharged PE) in this temperature range.

The experimental values for the permeation coefficient of water in PE at 1 atm and 298 K are 1.1×10^{-10} and 6.5×10^{-11} cm^2s^{-1} for LDPE and HDPE, respectively (□ in Fig. 11).[62, 66] Once again, these are the values after removing the effect of crystallinity. The simulated value is two orders of magnitude lower than experiments. This is due to the fact that the simulated solubility coefficient is two orders of magnitude lower than experimental values.

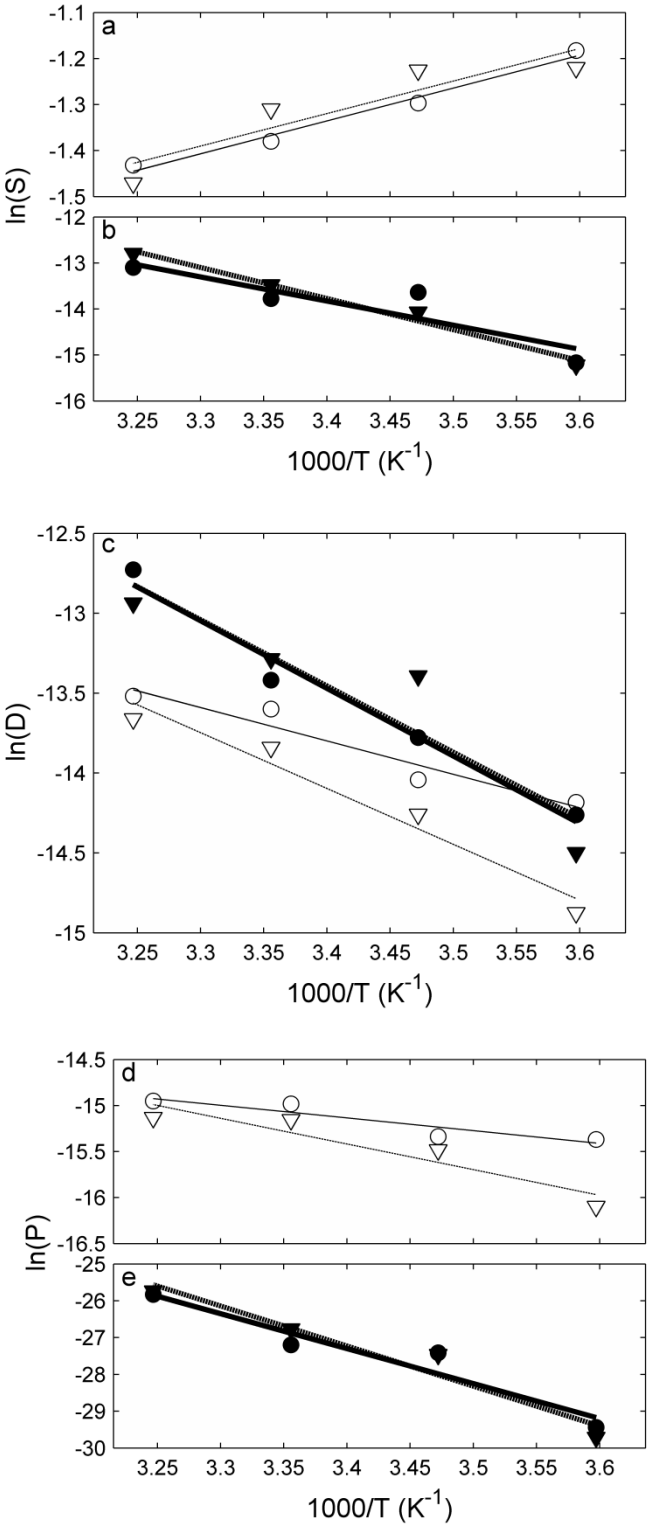

Figure 12: Temperature dependence plots of simulated a-b) solubility, c) diffusion and d-e) permeability coefficients of oxygen (open symbols) and water (filled symbols), in uncharged (circles) and charged (triangles) PE. Least squares linear regression to the values are shown with solid (uncharged) and dashed (charged) lines

Temperature dependence

The temperature dependence of solubility, diffusion and permeability coefficients are plotted in Fig. 12. Dissolution of oxygen in PE is exothermic, with a heat of solution of ΔH_S = -6 kJ/mol (both charged and uncharged systems)

Table 2 Heats of solution and diffusion and permeation activation energies of oxygen and water in PE.

	Comments	T (K)	ΔH_S (kJ/mol)	E_D (kJ/mol)	E_P (kJ/mol)	Reference
Oxygen	Uncharged / Charged	278–308	-6 / -6	13 / 25	8 / 20	This work
	Simulation	241–301	-	6.4	-	20
	Simulation	300-450	-15	32	17	14
	LLDPE	293–323	26 [a]	11	37	12
	LLDPE	277–333	28	2.4	31	9
	LLDPE [b]	298–323	-7.2/1.8/-9.2 [a]	45.6/33.5/46.8	38.4/35.3/37.6	64
	LLDPE [b]	323–358	-16.4/-0.6/-18.8 [a]	44.2/25.5/47.1	27.8/24.9/28.3	64
	LDPE	278–328	2.5	40.2	42.7	4, 5
	HDPE	278–328	-1.7	36.8	35.1	4, 5
	-	283–313	-0.66	1.9	1.2	8
	-	313–333	72	74	146	8
	-	293–333	113.37	-4.83	108.54	3
Water	Uncharged / Charged	278–308	44 / 56	30 / 36	75 / 93	This work
	LDPE	298-333	38 [c]	38 [c]	75 [c]	6
	LDPE	283–363	-	-	33.5	61
	LDPE	287–318	-	-	31	63

LLDPE = linear low density polyethylene, LDPE = low density polyethylene, HDPE = high density polyethylene, [a]Calculated from $E_P = E_D + \Delta H_S$. [b]Film prepared in three different ways cf. reference [64]. [c]Calculated from formula in reference.

Experimental heats of solution are given in Table 2. It is evident that comparison of the simulated and experimental values for oxygen is hindered by the large discrepancy in the experimental data. Several experiments have shown a dramatic change in ΔH_S at ~313 K [8, 9, 12]. The most pronounced discontinuity was found by Mrkić *et al.* where the heat of solution increased from –0.66 kJ/mol to 72 kJ/mol[8]. This discontinuity has not been observed in the present study, which may be due to the fact that the highest temperature studied here is 308 K. However, this effect was not observed in previous simulations of oxygen in PE over with a wider temperature range either[14]. In agreement with the simulations performed in this work, the previous simulations yielded an exothermic dissolution. The discontinuity in the temperature dependence from experimental studies was explained by the melting of the crystal regions at higher temperatures, and an α-transition,[12] which results in the relaxation of the crystalline regions hence releasing amorphous chains that were bonded to the crystalline regions.[67] This may also explain why the discontinuity is not observed in computational studies, where purely amorphous systems are studied.

The simulated heats of solution for water in PE (Table 2) are 44 kJ/mol (neutral force field) and 56 kJ/mol (charged force field), which shows that water dissolution in PE is an endothermic process. This is in agreement with the experimental data. The simulated and experimental heats of solution are also in reasonable agreement. The different behaviour of oxygen and water is probably due to the different bulk phases of the penetrant (oxygen is gas and water is liquid), as discussed above.

Similarly to the heats of solution, there is also a large variation in the experimentally determined diffusion

and permeation activation energies of oxygen. Nonetheless, as shown in Table 2, the simulated values of the diffusion activation energies, which are 13 kJ/mol (neutral force field) and 25 kJ/mol (charged force field), and the permeation activation energies, which are 8 and 20 kJ/mol, respectively, are in good agreement with most experimental measurements.

The simulated diffusion activation energies for water in PE are 30 kJ/mol (neutral force field) and 36 kJ/mol (charged force field), which are of the same magnitude as the diffusion activation energies for oxygen. The permeation activation energies for water are 75 and 93 kJ/mol for the neutral and charged systems, respectively. This is in very good agreement with some experiments [6] and twice as large as other experiments [66, 68].

Conclusions

Gibbs ensemble Monte Carlo and molecular dynamics simulations have been performed to study the molecular-level mechanism of oxygen and water permeation through polyethylene (PE) as well as the solubility, diffusion and permeation coefficients of these penetrants. A pressure of 1 atm was used in the simulations and the temperature ranged from 270 to 308 K. The AMBER force field, either with neutral atoms or with atomic charges obtained using the AM1-BCC method, was used for the simulations since it reproduced the experimental density of amorphous PE. It was found that including the charges in the force field does not have a large effect on the results.

Both the oxygen and water molecules diffuse through the PE via large amplitude, infrequent jumps, with the average size of the water jumps being smaller than for the oxygen. In addition, the diffusion coefficients of oxygen and water were similar in magnitude, although the increase in the diffusion coefficient as a function of temperature was larger for water than for oxygen. This is due to the larger activation barrier for diffusion of water through PE than for oxygen.

The solubility coefficient of oxygen in PE is six orders of magnitude larger than that of water. Hence, since the diffusion coefficients of oxygen and water are similar, the permeation of oxygen is also 5-6 orders of magnitude larger than that of water.

The large diversity in experimental data hinders comparison with the simulated data. However, there is qualitative, and even semi-quantitative, agreement between the simulated results and most of the experimental data. For example, in agreement with most experiments, the simulations show that the diffusion coefficients of oxygen and water are similar in magnitude and that the solubility and permeation coefficients of oxygen in PE are orders of magnitude higher than for water. In addition, dissolution of oxygen in PE is exothermic, whereas it is endothermic for water. Moreover, the activation barriers for oxygen diffusion and permeation through PE are smaller than for water.

Acknowledgements

The authors are very grateful for funding from the Swedish Knowledge Foundation (KK-stiftelsen). The simulations were performed on resources provided by the Swedish National Infrastructure for Computing

(SNIC) at High Performance Computing Center North (HPC2N) and Uppsala Multidisciplinary Center for Advanced Computational Science (UPPMAX) in Umeå and Uppsala, respectively.

References

1. Neburchilov V, Martin J, Wang H, and Zhang J. J. Power Sources 2007;169(2):221-238.
2. Bernardo P, Drioli E, and Golemme G. Ind Eng Chem Res 2009;48(10):4638-4663.
3. Gajdoš J, Galić K, Kurtanjek Ž, and Ciković N. Polymer Testing 2000;20(1):49-57.
4. Michaels AS and Bixler HJ. J Polym Sci 1961;50(154):393-412.
5. Michaels AS and Bixler HJ. J Polym Sci 1961;50(154):413-439.
6. McCall DW, Douglass DC, Blyler LL, Johnson GE, Jelinski LW, and Bair HE. Macromolecules 1984;17(9):1644-1649.
7. Compañ V, López-Lidón M, Andrio A, and Riande E. Macromolecules 1998;31(20):6984-6990.
8. Mrkić S, Galić K, Ivanković M, Hamin S, and Ciković N. J. Appl. Polym. Sci. 2006;99(4):1590-1599.
9. Kurek M, Klepac D, Ščetar M, Galić K, Valić S, Liu Y, and Yang W. Polym Bull 2011;67(7):1293-1309.
10. Jean YC. Microchem. J. 1990;42(1):72-102.
11. Hodge RM, Bastow TJ, Edward GH, Simon GP, and Hill AJ. Macromolecules 1996;29(25):8137-8143.
12. Compañ V, Ribes A, Díaz-Calleja R, and Riande E. Polymer 1996;37(11):2243-2250.
13. Schatzberg P. J. Phys. Chem. 1963;67(4):776-779.
14. Gestoso P and Karayiannis NC. J. Phys. Chem. B 2008;112(18):5646-5660.
15. Tamai Y, Tanaka H, and Nakanishi K. Macromolecules 1994;27(16):4498-4508.
16. Pant PVK and Boyd RH. Macromolecules 1993;26(4):679-686.
17. Fukuda M. J. Chem. Phys. 2000;112(1):478-486.
18. Tamai Y, Tanaka H, and Nakanishi K. Macromolecules 1995;28(7):2544-2554.
19. Fukuda M and Kuwajima S. J. Chem. Phys. 1997;107(6):2149-2159.
20. Takeuchi H and Okazaki K. J. Chem. Phys 1990;92(9):5643-5652.
21. Cozmuta I, Blanco M, and Goddard WA. The Journal of Physical Chemistry B 2007;111(12):3151-3166.
22. Sok RM, Berendsen HJC, and van Gunsteren WF. J. Chem. Phys. 1992;96(6):4699.
23. Michaels AS and Parker RB. J Polym Sci 1959;41(138):53-71.
24. Norman GE and Filinov VS. High Temperature 1969;7(7):216-222.
25. Panagiotopoulos AZ. Molecular Physics: An International Journal at the Interface Between Chemistry and Physics 1987;61(4):813 - 826.
26. Panagiotopoulos AZ, Quirke N, Stapleton M, and Tildesley DJ. Molecular Physics: An International Journal at the Interface Between Chemistry and Physics 1988;63(4):527 - 545.
27. Cornell WD, Cieplak P, Bayly CI, Gould IR, Merz KM, Ferguson DM, Spellmeyer DC, Fox T, Caldwell JW, and Kollman PA. Journal of the American Chemical Society 1995;117(19):5179-5197.
28. Mayo SL, Olafson BD, and Goddard WA. J. Phys. Chem. 1990;94(26):8897-8909.
29. Jorgensen WL, Maxwell DS, and Tirado-Rives J. Journal of the American Chemical Society 1996;118(45):11225-11236.
30. MacKerell AD, Bashford D, Bellott, Dunbrack RL, Evanseck JD, Field MJ, Fischer S, Gao J, Guo H, Ha S, Joseph-McCarthy D, Kuchnir L, Kuczera K, Lau FTK, Mattos C, Michnick S, Ngo T, Nguyen DT, Prodhom B, Reiher WE, Roux B, Schlenkrich M, Smith JC, Stote R, Straub J, Watanabe M, Wiórkiewicz-Kuczera J, Yin D, and Karplus M. The Journal of Physical Chemistry B 1998;102(18):3586-3616.
31. Karlsson GE, Johansson TS, Gedde UW, and Hedenqvist MS. Journal of Macromolecular Science, Part B 2002;41(2):185-206.
32. Zhang J, Liang Y, Yan JZ, and Lou JZ. Polymer 2007;48(16):4900-4905.
33. McAliley JH and Bruce DA. J. Chem. Theor. Comput. 2011;7(11):3756-3767.
34. Bayly CI, Cieplak P, Cornell W, and Kollman PA. J. Phys. Chem. 1993;97(40):10269-10280.
35. Dupradeau F-Y, Pigache A, Zaffran T, Savineau C, Lelong R, Grivel N, Lelong D, Rosanski W, and Cieplak P. Phys. Chem. Chem. Phys. 2010;12(28):7821-7839.
36. GAMESS (US). http://www.msg.chem.iastate.edu/gamess/index.html: Iowa State University Quantum Chemistry Group, 2007.
37. Jakalian A, Jack DB, and Bayly CI. J. Comput. Chem. 2002;23(16):1623-1641.
38. Jakalian A, Bush BL, Jack DB, and Bayly CI. J. Comput. Chem. 2000;21(2):132-146.
39. Stewart JJP. MOPAC2009. Colorado Springs, CO, USA: Stewart Computational Chemistry, 2009.
40. Fischer J and Lago S. J. Chem. Phys. 1983;78(9):5750-5758.
41. Reiher WE. Theoretical studies of hydrogen bonding. PhD Thesis: Harvard University, 1985.
42. Price DJ and Brooks Iii CL. J. Chem. Phys 2004;121(20):10096-10103.
43. Johansson E, Bolton K, Theodorou DN, and Ahlstrom P. J. Chem. Phys. 2007;126(22):224902.
44. Allen G, Gee G, and Wilson GJ. Polymer 1960;1(0):456-466.
45. Martin MG. MCCCS Towhee. http://towhee.sourceforge.net, 2011.
46. Plimpton S. J. Comput. Phys. 1995;117(1):1-19.
47. LAMMPS http://lammps.sandia.gov, 2011.
48. MAPS. Paris, France: SCIENOMICS SARL, 2012.
49. Bolton K and Nordholm S. J. Comput. Phys. 1994;113(2):320-335.
50. Frenkel D and Smit B. Understanding Molecular Simulation: from algorithms to applications, 2nd ed.: Academic Press, 2002.
51. Neusius T, Sokolov IM, and Smith JC. Phys. Rev. E 2009;80(1):011109.
52. Metzler R and Klafter J. Physics Reports 2000;339(1):1-77.
53. van der Vegt NFA and Briels WJ. J. Chem. Phys. 1998;108(22):9558.
54. Müller-Plathe F, Rogers SC, and van Gunsteren WF. J. Chem. Phys. 1993;98(12):9895.
55. Efron B. Annals of Statistics 1977;7(1):1-26.
56. Efron B and Tibshirani R. Statistical Science 1986;1(1):54-75.
57. Yasuda H. J. Appl. Polym. Sci. 1975;19(9):2529-2536.
58. Johansson E, Bolton K, Theodorou DN, and Ahlstrom P. J. Chem. Phys. 2007;127(19):191101.
59. Johansson E, Ahlström P, and Bolton K. Polymer 2008;49(24):5357-5362.
60. Holden PS, Orchard GAJ, and Ward IM. J Polym Sci Pol Phys 1985;23(4):709-731.
61. Kanehashi S, Kusakabe A, Sato S, and Nagai K. J Membrane Sci 2010;365(1–2):40-51.
62. Myers AW, Meyer JA, Rogers CE, Stannett V, and Szwarc M. Tappi 1961;44:58-64.
63. Massey LK. Permeability Properties of Plastics and Elastomers - A Guide to Packaging and Barrier Materials (2nd Edition): William Andrew Publishing/Plastics Design Library, 2003.
64. Boyd RH. J. Polym. Sci., Polym. Phys. Ed. 1983;21(4):505-514.
65. Riddick JA, Bunger WB, and Sakano TK. Organic solvents : physical properties and methods of purification, 4th ed. New York: Wiley, 1986.
66. Pauly S. Permeability and Diffusion Data In: Brandrup J, Immergut EH, Grulke EA, Abe A, and Bloch DR, editors. Polymer Handbook John Wiley & Sons.,

1999. pp. VI/543-VI/569.
67. Boyd RH. Polymer Engineering & Science 1979;19(14):1010-1016.
68. Hamilton RL. Bell Syst. Tech. J. 1967;46(2):391-415.